



AFRL-RY-WP-TR-2011-1045

INNOVATIVE SOLID STATE INFRARED LASER DEVICES

Kenneth L. Schepler

**Electro-Optical Countermeasures Technology Branch
Multispectral Sensing & Detection Division**

**DECEMBER 2010
Final Report**

Approved for public release; distribution unlimited.

See additional restrictions described on inside pages

STINFO COPY

**AIR FORCE RESEARCH LABORATORY
SENSORS DIRECTORATE
WRIGHT-PATTERSON AIR FORCE BASE, OH 45433-7320
AIR FORCE MATERIEL COMMAND
UNITED STATES AIR FORCE**

NOTICE AND SIGNATURE PAGE

Using Government drawings, specifications, or other data included in this document for any purpose other than Government procurement does not in any way obligate the U.S. Government. The fact that the Government formulated or supplied the drawings, specifications, or other data does not license the holder or any other person or corporation; or convey any rights or permission to manufacture, use, or sell any patented invention that may relate to them.

This report was cleared for public release by the USAF 88th Air Base Wing (88 ABW) Public Affairs Office (PAO) and is available to the general public, including foreign nationals. Copies may be obtained from the Defense Technical Information Center (DTIC) (<http://www.dtic.mil>).

AFRL-RY-WP-TR-2011-1045 HAS BEEN REVIEWED AND IS APPROVED FOR PUBLICATION IN ACCORDANCE WITH ASSIGNED DISTRIBUTION STATEMENT.

*//Signature//

KENNETH L. SCHEPLER
EO CM Tech Branch
Multispectral Sensing & Detection Division

//Signature//

JOHN F. CARR, Chief
EO CM Tech Branch
Multispectral Sensing & Detection Division

//Signature//

TRACY W. JOHNSTON
Multispectral Sensing & Detection Division
Sensors Directorate

This report is published in the interest of scientific and technical information exchange, and its publication does not constitute the Government's approval or disapproval of its ideas or findings.

*Disseminated copies will show “//Signature//” stamped or typed above the signature blocks.

REPORT DOCUMENTATION PAGE				Form Approved OMB No. 0704-0188	
<p>The public reporting burden for this collection of information is estimated to average 1 hour per response, including the time for reviewing instructions, searching existing data sources, gathering and maintaining the data needed, and completing and reviewing the collection of information. Send comments regarding this burden estimate or any other aspect of this collection of information, including suggestions for reducing this burden, to Department of Defense, Washington Headquarters Services, Directorate for Information Operations and Reports (0704-0188), 1215 Jefferson Davis Highway, Suite 1204, Arlington, VA 22202-4302. Respondents should be aware that notwithstanding any other provision of law, no person shall be subject to any penalty for failing to comply with a collection of information if it does not display a currently valid OMB control number. PLEASE DO NOT RETURN YOUR FORM TO THE ABOVE ADDRESS.</p>					
1. REPORT DATE (DD-MM-YY) December 2010		2. REPORT TYPE Final		3. DATES COVERED (From - To) 01 October 2005 – 30 September 2010	
4. TITLE AND SUBTITLE INNOVATIVE SOLID STATE INFRARED LASER DEVICES				5a. CONTRACT NUMBER In-house	
				5b. GRANT NUMBER	
				5c. PROGRAM ELEMENT NUMBER 61102F/62204F	
6. AUTHOR(S) Kenneth L. Schepler				5d. PROJECT NUMBER 2003	
				5e. TASK NUMBER 12	
				5f. WORK UNIT NUMBER 20031224	
7. PERFORMING ORGANIZATION NAME(S) AND ADDRESS(ES) Electro-Optical Countermeasures Technology Branch (AFRL/RYMW) Multispectral Sensing & Detection Division Air Force Research Laboratory, Sensors Directorate Wright-Patterson Air Force Base, OH 45433-7320 Air Force Materiel Command, United States Air Force				8. PERFORMING ORGANIZATION REPORT NUMBER AFRL-RY-WP-TR-2011-1045	
9. SPONSORING/MONITORING AGENCY NAME(S) AND ADDRESS(ES) Air Force Research Laboratory Sensors Directorate Wright-Patterson Air Force Base, OH 45433-7320 Air Force Materiel Command United States Air Force				10. SPONSORING/MONITORING AGENCY ACRONYM(S) AFRL/RYMW	
				11. SPONSORING/MONITORING AGENCY REPORT NUMBER(S) AFRL-RY-WP-TR-2011-1045	
12. DISTRIBUTION/AVAILABILITY STATEMENT Approved for public release; distribution unlimited.					
13. SUPPLEMENTARY NOTES PAO Case Number: 88ABW-11-0032; Clearance Date: 05 Jan 2011. This report contains color.					
14. ABSTRACT Technology and devices were investigated that can improve lasing power and efficiency, extend tunability, create and modulate laser waveforms, and provide versatile performance. Reliability, cost, and suitability to the military environment were addressed along with technical performance. Cr ²⁺ :ZnSe laser power was scaled up to 14 W CW. Tunable Cr ²⁺ :ZnSe lasing over 2275-2700 nm was achieved with grating tuning and powers ranging from 2 to 9 W. Passive saturable absorber modelocking was achieved with several hundred mW of output power. Gain switched Cr ²⁺ :ZnSe lasing generated 3 mJ of output energy with 52% slope efficiency. Efforts to fabricate a Cr:ZnSe fiber core using the RIT method were unsuccessful. More promising techniques include deposition of ZnSe in the hollow core of a silica fiber and fabrication of waveguide structures in ZnSe using ultrashort pulses. Sub-nanosecond pulses were generated using a μ -chip Nd laser oscillator and an Yb-doped fiber amplifier. Wavelengths were converted to the mid-IR using nonlinear frequency conversion. An alternative Tm:YAG microchip laser that operates directly in the infrared spectral region was investigated. CW Tm lasing was achieved but passive Q-switched was not. An image processing technique was used to provide quantitative evaluation of poling quality of quasi-phase matched crystals. The mapping of calculated d _{eff} to threshold matched the nonlinear optical parametric generation measurements quite well.					
15. SUBJECT TERMS infrared lasers, laser tuning					
16. SECURITY CLASSIFICATION OF:			17. LIMITATION OF ABSTRACT: SAR	18. NUMBER OF PAGES 44	19a. NAME OF RESPONSIBLE PERSON (Monitor) Kenneth L. Schepler 19b. TELEPHONE NUMBER (Include Area Code) N/A
a. REPORT Unclassified	b. ABSTRACT Unclassified	c. THIS PAGE Unclassified			

Table of Contents

List of Figures	ii
Acknowledgements	iii
1. Summary	1
1.1 Objective	1
1.2 Approach	1
1.3 Accomplishments	1
2. Introduction	2
2.1 Background	2
2.2 Program Tasks	2
3. Results and Discussion	4
3.1 Development of tunable, solid-state mid-infrared lasers	4
3.1.1 Cr ²⁺ :ZnSe power scaling	4
3.1.2 Cr ²⁺ modelocking	5
3.1.3 Gain switched laser	8
3.1.4 Waveguide devices for thermal lensing mitigation	10
3.2 Development of sub-nanosecond IR source	12
3.2.1 Nd μ -chip laser with PPLN frequency conversion	12
3.2.2 Tm:YAG μ -chip laser	13
3.3 Characterization of poled materials using digital image processing	19
3.3.1 Methodology	21
3.3.2 Experimental OPG test	23
3.3.3 Image processing conclusions	25
4. Conclusions	26
5. Recommendations	27
6. References	28
7. List of Publications and Presentations	30
8. List of Acronyms, Abbreviations, and Symbols	32

List of Figures

Figure	Page
Figure 1. Cr ²⁺ :ZnSe MOPA configuration for an L cavity design.	5
Figure 2. Cr ²⁺ :ZnSe MOPA performance. Dashed lines are experimental measurements. Solid lines are modeling calculations.	5
Figure 3. z-cavity resonator. Used for tuning with a grating (G) and or modelocking with a focusing mirror substituting for the grating and a saturable absorber (SA).	6
Figure 4: Q-switched envelope with weak modelocking at 150 mW output.....	7
Figure 5. Cr ²⁺ :ZnSe modelocked pulse train.	8
Figure 6. Absorption spectra of Cr:ZnSe gain elements (left) and their photograph (right).	8
Figure 7. Cavity design for gain-switched laser.	9
Figure 8. Cr ²⁺ :ZnSe laser gain-switched output vs. absorbed pump energy for output mirrors with 50% and 70% reflectivity.	9
Figure 9. Gain-switched Cr ²⁺ :ZnSe temporal profile where the 70% reflective outcoupler trace is offset for clarity (left), and spatial profile when focused to a 265 μm spot radius (right)... ..	10
Figure 10. Spectral content of gain-switched Cr ²⁺ :ZnSe laser output. (left) Complete spectra showing no 2.095 μm pump present, (right) zoomed in to show peak emission and linewidth.	10
Figure 11. Cr:ZnSe RIT core in silica fiber preform.	11
Figure 12. Tm ³⁺ energy levels. Each labeled level is actually a manifold of levels split by spin-orbit.....	14
Figure 13. Tm ³⁺ :YAG absorbance, not corrected for surface reflectivities.....	15
Figure 14. Tm:YAG absorbance in the diode pump region for 3% and 6% Tm doping....	15
Figure 15. Tm:YAG emission not corrected for spectrometer response.	16
Figure 16. Diagram of 2-μm short pulse laser source.....	17
Figure 17. Tm:YAG CW microchip laser power.....	18
Figure 18. Typical etched lithium niobate test sample image.	22
Figure 19. Binary map of domain structure.	22
Figure 20. Fourier transform of map at row 1000 using various levels of zero-padding.	23
Figure 21. Calculated and measured threshold of PPLN crystal in an OPG setup.....	24

Acknowledgements

The author gratefully acknowledges funding for this research from the Air Force Office of Scientific Research (AFOSR) and the Air Force Research Laboratory Sensors Directorate (AFRL/RY).

I also gratefully acknowledge the diligent effort of my associates and students listed below who performed the research reported here.

Staff and Advisors

Dr Rita Peterson	AFRL/RY
Dr Patrick Berry	AFRL/RY
Mr George Tietz	AFRL/RY (retired)
Capt Tim Calver	AFRL/RY
Capt David Whelan	AFRL/RY
Capt Mike Plourde	AFRL/RY
2Lt Ryan Meeter	AFRL/RY
Prof Peter Powers	University of Dayton
Prof Ivan Lima	North Dakota State University (summer faculty)
Dr Shrikrishna Hegde	University of Dayton Research Institute
Mr John McCurdy	OptiMetrics, Inc.

Students

Major Torrey Wagner, PhD	(AFIT) AFRL/RD
Mr Matt Cocuzzi	(University of Dayton) AFRL/RY
Mr Charles Phelps	(University of Dayton) AFRL/RY
Mr Jonathan Evans	(AFIT) AFRL/RY
Mr Jim Alverson	(University of Dayton) AFRL/RY

1. Summary

This technical report summarizes the results of in-house workunit 20031224 entitled “Innovative Solid-State Infrared Devices.” The workunit was funded by AFOSR (Dr Howard Schlossberg, Program Manager) under Program Element 61102F and by the Sensors Directorate under Program element 62204F. The workunit spanned five fiscal years (FY06-FY10).

1.1 Objective

This in-house effort developed advanced infrared laser materials and architectures, tunable infrared laser devices and other ancillary technologies. Technology and devices were investigated that can improve lasing power and efficiency, extend lasing tunability, create and modulate laser waveforms, and provide versatile laser performance. Reliability, cost, and suitability to the military environment were addressed along with technical performance. Emphasis was placed upon technology transfer from basic research to demonstration of application-based devices. Potential military applications include infrared countermeasures for aircraft self-protection, laser radar for target identification, remote sensing of chemical and biological agents, and high speed communications.

1.2 Approach

The approach concentrated on developing advanced lasing, frequency conversion, and beam control capabilities. Emphasis was placed on demonstrating novel techniques that will improve the performance, reliability, and maturity of active infrared materials and devices. Advanced infrared materials were developed and transitioned into breadboard devices. Our focus was upon fiber lasers for efficiency, conformability, reliability, and as a first step toward the elimination of free-space transmission and the reduction of the number of optical components in operational systems. Infrared wavelengths at ~10-W powers in the 2-5 μm and 8-12 μm regions with room temperature devices were performance goals. This in-house workunit was closely aligned with in-house WU 20031225 which develops nonlinear materials and devices for infrared frequency conversion.

1.3 Accomplishments

Accomplishments in the development of mid-IR laser source are summarized in this final report with references provided to details published in journals, conference proceedings or technical reports.

2. Introduction

2.1 Background

The USAF makes extensive use of electromagnetic radiation for sensing applications. Active defense of aircraft from heat-seeking missiles requires laser sources that can be tuned throughout the 2-5 μm spectral region, or at least throughout wavelength bands that are transmitted through the atmosphere. Other military applications of mid-IR laser sources include laser radar for target identification, remote sensing of chemical and biological agents, and high speed communications. Commercial applications in medicine, environmental sensing, industrial production and spectroscopy are also of interest.

2.2 Program Tasks

Research activities for this workunit were divided among the following tasks:

1. Tunable, solid-state mid-infrared lasers. This task includes materials that lase directly in the mid-infrared and offer the possibility of broadband tuning. Cr^{2+} ions doped into suitable hosts such as ZnSe were our main area of investigation. Versatile operation in the CW, long pulse, short pulse and ultrashort pulse temporal regimes was investigated in order to provide sources which address current IRCM needs as well as prepare for future threat scenarios involving imaging seeker systems. Agile waveform and high performance master oscillators were combined with high power amplifier systems to satisfy current and future system requirements. Devices developed in this task can be combined with nonlinear frequency conversion devices developed under WU 20031225 to cover the entire atmospheric transmission bands of 2-5 μm and 8-12 μm . Cost and reliability issues were emphasized as well as the technical issues of tunability and power scaling.
2. Short pulse mid-infrared lasers. This task includes demonstration of devices that achieve pulsed output in the mid-IR with high repetition rate and high average power. This was accomplished by combining novel high performance oscillators producing sub-nanosecond pulses at fixed wavelengths with cutting edge fiber amplification systems. Such devices are required for high resolution and high speed search and ID and can also be used as pump systems for nonlinear frequency conversion devices produced through WU 20031225 to generate pulses in a wide range of wavelength regions.
3. Nonlinear frequency conversion. Work on the development of mid-IR nonlinear frequency conversion devices was initially under the auspices of this workunit. In FY2007 we decided to breakout the nonlinear work into a new workunit with Dr Peterson as the technical lead when her proposal to expand the nonlinear work was approved. Because of this change, some early nonlinear work such as "Characterization of periodically poled nonlinear materials using digital image processing," published in AFRL-RY-WP-TM-2008-1205 [1] remained in this workunit but subsequent efforts are reported under workunit 20031225.

4. Additional areas of interest. This task includes work that does not fit under any of the other tasks, such as training and academic progress of students in the group, and facilities maintenance and upgrades. Cooperative solid-state laser research was performed with several universities in the areas of Cr^{2+} laser development, waveguide machining, and ZnSe fiber fabrication.

3. Results and Discussion

The primary objective of this workunit was to develop and demonstrate advanced mid-IR sources for military applications.

3.1 Development of tunable, solid-state mid-infrared lasers

IRCM for military aircraft requires mid-IR lasers that are robust, low-cost and efficient. Room temperature operation and broadband tunability are highly desirable. Versatility of laser output in terms of pulse width and repetition rate are also advantageous. Other applications like laser radar and remote sensing have similar requirements but often not as stringent with the exception of narrow bandwidth.

Cr^{2+} -doped chalcogenides are ideal mid-IR sources since they meet many of the above requirements. DeLoach et al. [2] demonstrated the first Cr^{2+} laser. Numerous investigators, including our own group, have continued the development of Cr^{2+} lasers in CW, gain-switched and modelocked modes of operation. Work performed under this workunit concentrated on scaling up the lasing power of $\text{Cr}^{2+}:\text{ZnSe}$, modelocked operation of $\text{Cr}^{2+}:\text{ZnSe}$ and suppression of thermal lensing effects.

3.1.1 $\text{Cr}^{2+}:\text{ZnSe}$ power scaling

We achieved first demonstration of a $\text{Cr}^{2+}:\text{ZnSe}$ Master Oscillator Power Amplifier (MOPA) using the setup shown in Figure 1 with record 14 W of CW output (Figure 2) for power scaling while maintaining beam quality (publication 1). We also demonstrated 2-9 W of CW output power tuning over a 400 nm range using a grating as the tuning element. In gain-switched operation we demonstrated a record 3.1 mJ pulse energy and 200 kW peak power for high pulse energy frequency conversion and increased laser radar range (See publications 1, 6-9 for further details).

Major factors in the advancement of $\text{Cr}^{2+}:\text{ZnSe}$ included new high-power pump lasers and improved $\text{Cr}^{2+}:\text{ZnSe}$ material quality. Tm-doped and Er-doped fiber lasers are now commercially available with > 100 W of output power with high beam quality. Use of such pump lasers makes $\text{Cr}^{2+}:\text{ZnSe}$ laser operation quite convenient and straightforward. Through the considerable efforts [3] of Prof Sergey Mirov at University of Alabama-Birmingham, $\text{Cr}^{2+}:\text{ZnSe}$ fabrication has advanced considerably. His efforts, funded by numerous agencies including AFRL, have resulted in the fabrication of material with low scattering loss and uniform doping of Cr^{2+} active ions. Laser material is commercially available from his spin-off company now owned by IPG Photonics.

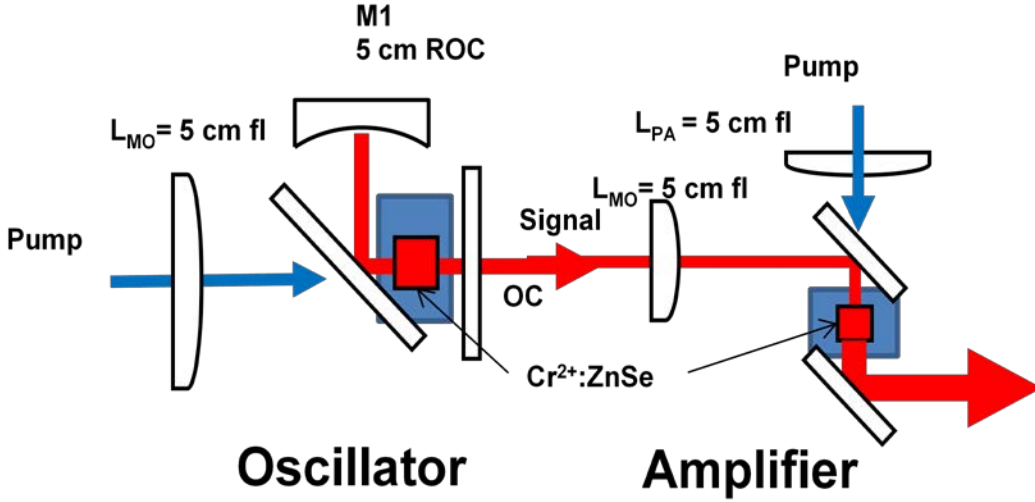


Figure 1. $\text{Cr}^{2+}:\text{ZnSe}$ MOPA configuration for an L cavity design.

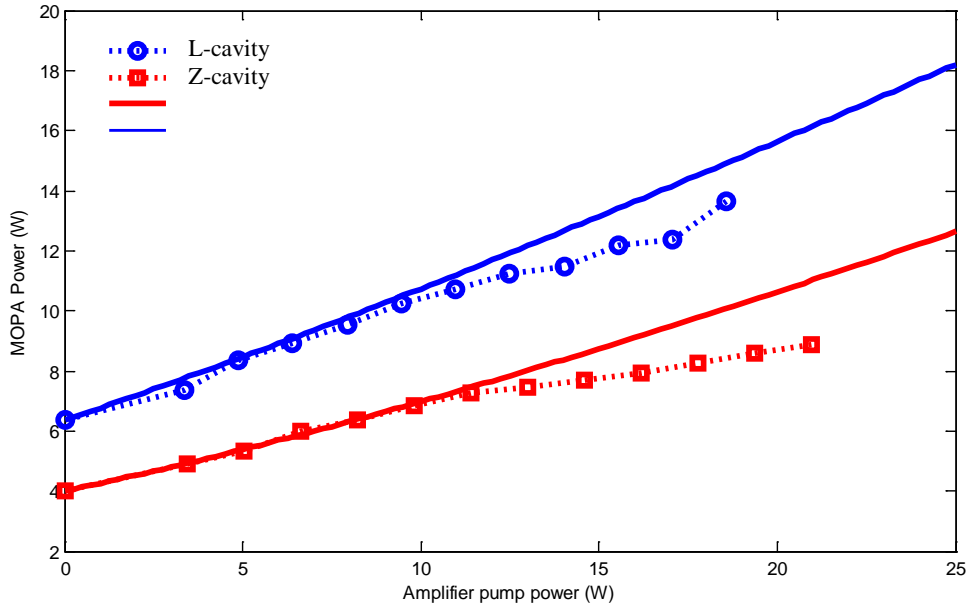


Figure 2. $\text{Cr}^{2+}:\text{ZnSe}$ MOPA performance. Dashed lines are experimental measurements. Solid lines are modeling calculations.

3.1.2 Cr^{2+} modelocking

Modelocked laser operation of $\text{Cr}^{2+}:\text{ZnSe}$ was first demonstrated [4] by Carrig *et al.* in 2000. They produced 4.4 ps pulses with 82 mW average power. Passive modelocking has been used to generate much shorter pulses with the record pulse width being 80 fs [5]. Our goal in this work was to achieve higher modelocked powers (> 1 W) without requiring sub-ps pulses.

We used a z-cavity resonator design shown in Figure 3 which was also used for high power CW operation with an HR mirror located at M2. Placing a grating at M2 provided broadband tuning.

By placing a focusing HR mirror at M2 and locating a saturable absorber at the focus we were able to achieve preliminary modelocking of $\text{Cr}^{2+}:\text{ZnSe}$.

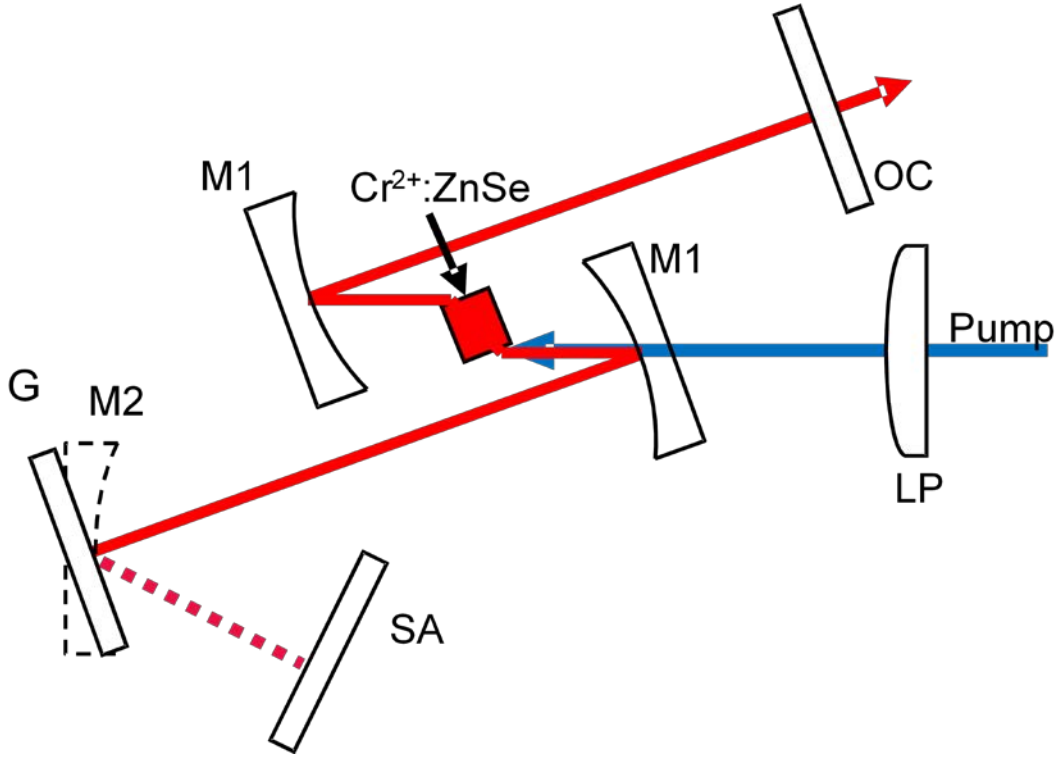


Figure 3. z-cavity resonator. Used for tuning with a grating (G) and or modelocking with a focusing mirror substituting for the grating and a saturable absorber (SA).

The modelocking cavity, shown schematically in Figure 3, consisted of two 5 cm radius of curvature (ROC) spherical mirrors (M1), AR-coated for 1908 nm pump radiation and HR-coated for the 2000-3000 nm spectral range, a 10 cm ROC HR mirror (M2), a flat sapphire 70% transmissive output coupler (OC) and a semiconductor saturable absorber mirror (SESAM) fabricated by NRL for this experiment. The polycrystalline, $8.9 \times 7.0 \times 3.0 \text{ mm}^3$ (LxWxH) $\text{Cr}^{2+}:\text{ZnSe}$ gain element was installed at the Brewster angle of 67.7° for horizontal polarization parallel to the plane of the optical table. The laser crystal was pumped along the long dimension with a linearly polarized IPG Tm-fiber laser with a maximum output of 37 W.

This configuration allowed for some adjustment of cavity fluence on the SA simply by changing the location of the SA. This cavity initially produced Q-switching behavior which was thought to contain modelocked pulses. Upon further investigation, we determined that this behavior was caused by beating between modes or “mode beating” as opposed to modelocking. This can happen when modelocking is not strong; multiple modes are present but they are not locked together in phase. Figure 4 shows Q-switched envelopes with a $2 \mu\text{s}$ period or 500 kHz repetition rate. Closer looks at the 100 ns/div and 10 ns/div scale show some indication of pulses occurring at the expected $\sim 400 \text{ MHz}$ rate.

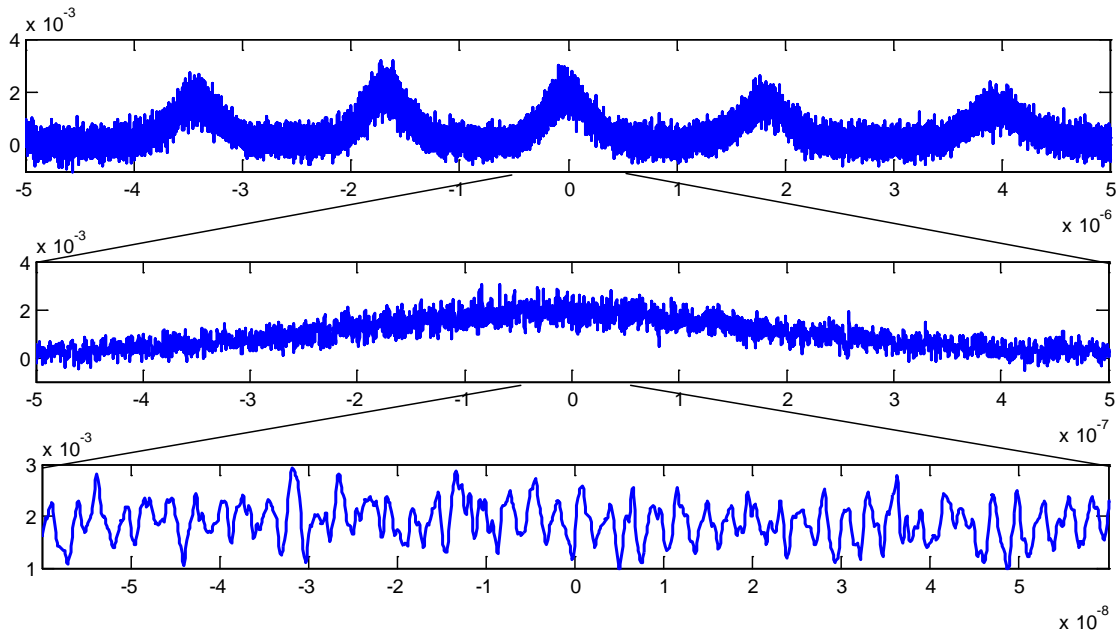


Figure 4: Q-switched envelope with weak modelocking at 150 mW output.

Modeling was conducted for our specific cavity ($R=70\%$ outcoupler) and it was found that Q-switched modelocking instability is expected to occur. A paper by Hoenninger et al. [6] defines a critical intra-cavity pulse energy as the threshold for Q-switched modelocking instability. To avoid this instability, the intra-cavity pulse energy can be increased by increasing the pump power, raising the output coupler reflectivity or increasing the cavity length. The easiest method in our case was to raise the output coupler reflectivity to 90%. This produced pulses (using a Boston Electronics / VIGO detector) which were orders of magnitude stronger than the previous output and were viewable on a high-speed oscilloscope (LeCroy WaveRunner 204MXi) running at 2 GHz bandwidth with $50\ \Omega$ coupling as shown in Figure 5 below.

The next steps in this research will be further stabilization of the cavity output, autocorrelation of the pulses to measure pulse width as well as proving that we do have modelocking, and frequency resolved optical gating (FROG) to determine the phase as well as the magnitude of the pulses.

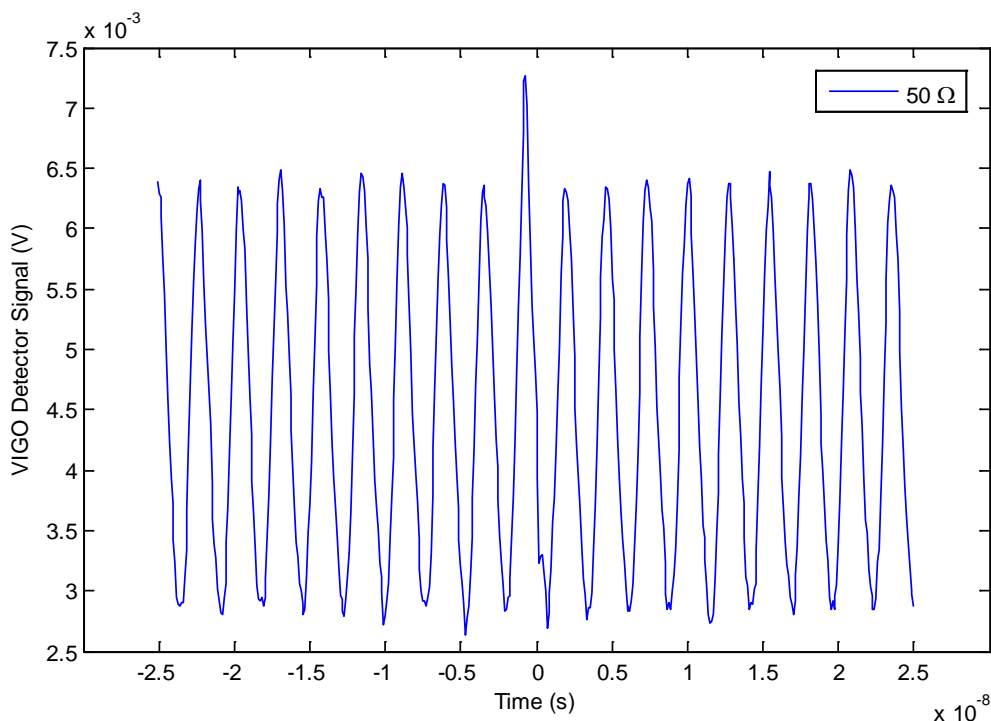


Figure 5. $\text{Cr}^{2+}:\text{ZnSe}$ modelocked pulse train.

Already, we have observed output powers of several hundred milliwatts which is more power than others have achieved when modelocking $\text{Cr}^{2+}:\text{ZnSe}$ and has us well along the path towards a multi-watt modelocked laser operating in-band for IRCM applications.

3.1.3 Gain switched laser

The 6-8 μs lifetime of $\text{Cr}:\text{ZnSe}$ is too short for Q-switching. However, it is possible to gain-switch the material using short pump pulses. In this study we used Brewster cut $\text{Cr}:\text{ZnSe}$ gain elements fabricated by IPG Photonics Corporation with a peak absorption coefficient (α) of 8-9 cm^{-1} at 1.78 μm , and $\alpha = 1 \text{ cm}^{-1}$ at 2.1 μm wavelengths. Currently developed technology allows fabrication of large ($5 \times 5 \times 50 \text{ mm}^3$) uniformly doped crystals. Figure 6 shows the fabricated gain elements and their measured absorption spectra.

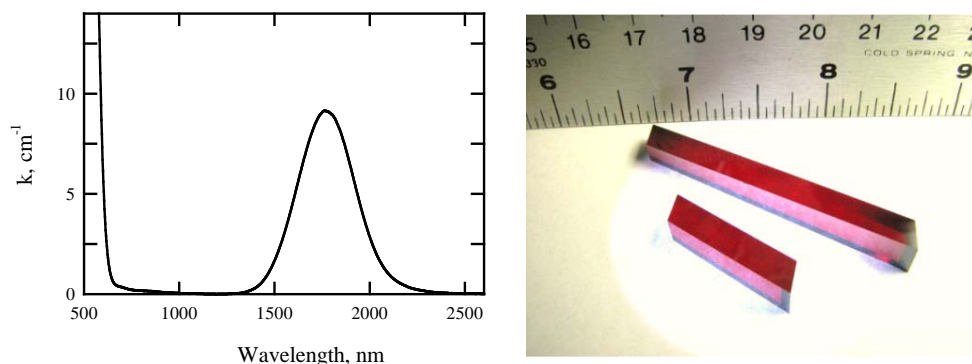


Figure 6. Absorption spectra of $\text{Cr}:\text{ZnSe}$ gain elements (left) and their photograph (right).

The pump source used for our gain-switched Cr:ZnSe laser experiments was a Cr,Tm,Ho:YAG laser (Schwartz Electro-Optics, SEO). The laser pulse FWHM was 90 ns, and pulse characteristics include a wavelength of 2.095 μm and up to 13 mJ of pulse energy.

In the resonator design shown in Figure 7, $M1$ is a 50 cm ROC mirror, d_1 is 7.5 cm, d_2 is 15 cm and the mode size was adjustable with a variable length d_1 . Calculations predicted a $1/e^2$ mode radius of 600 μm at the planar outcoupler and 450 μm at the planar $M2$ folding mirror. The pump was focused to a $\sim 500 \mu\text{m}$ spot radius on the crystal using a 1 meter focal length lens placed 30 cm away. We used a sample which was 24 mm long, 4.7 mm high and tapered from 6.3 to 5.3 mm wide to prevent parasitic oscillations in the transverse direction.

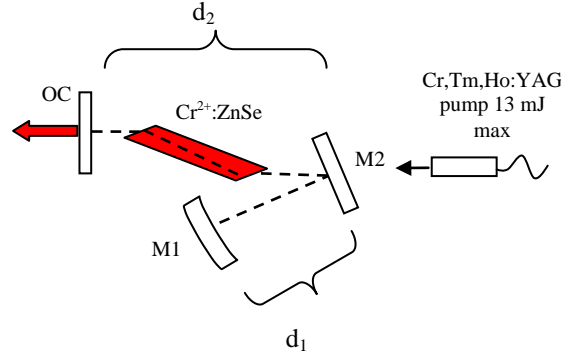


Figure 7. Cavity design for gain-switched laser.

5ER.

Cr:ZnSe pulse energies using 50% and 70% outcouplers are presented in Figure 8 along with their slope efficiencies. Measurement of unabsorbed pump energy was performed over the range of pump powers by recording the laser output after dumping the Cr^{2+} emission away with a dichroic mirror. This unabsorbed pump energy varied from 5-15% of incident energy, and was subtracted from the incident pulse energy to yield the *absorbed pump* x-axis in Figure 8. With the 50% outcoupler, maximum pulse energy achieved was 3 mJ with 52% slope efficiency. The 70% outcoupler had less (36%) slope efficiency but a lower threshold (3 mJ vs 5 mJ).

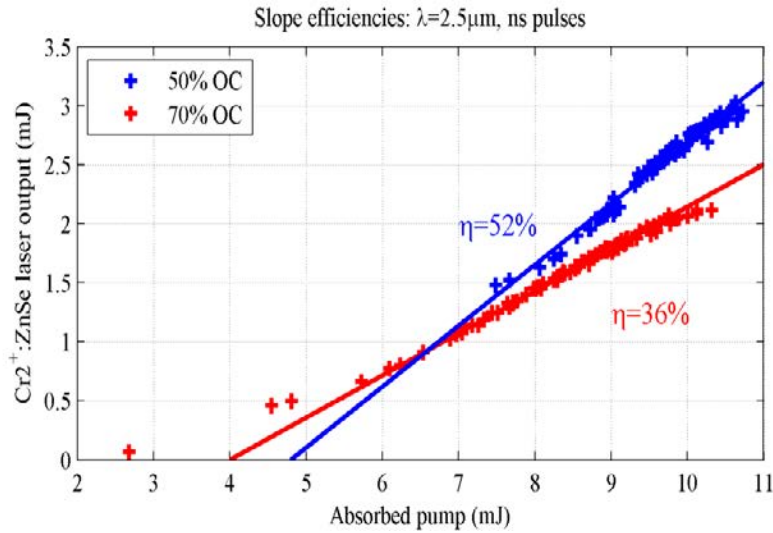


Figure 8. Cr^{2+} :ZnSe laser gain-switched output vs. absorbed pump energy for output mirrors with 50% and 70% reflectivity.

The gain-switched temporal profiles are shown in Figure 9 (left) for the 50% and 70% outcouplers. Two peaks are generated under the pump envelope; FWHM of the larger of the two peaks is ~ 10 ns. As the outcoupler reflectivity is reduced, the amount of energy in the secondary peak is shifted towards the primary peak. For this laser, a beam quality of $M^2 = 1.4$ was measured for both x and y axes, with a slight astigmatism. Figure 9 (right) shows that the beam has a near-Gaussian spatial profile when focused to a $265 \mu\text{m}$ spot radius.

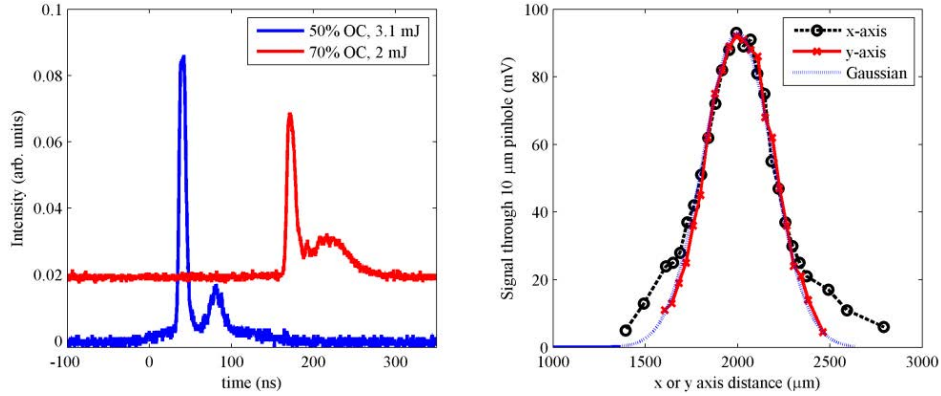


Figure 9. Gain-switched $\text{Cr}^{2+}:\text{ZnSe}$ temporal profile where the 70% reflective outcoupler trace is offset for clarity (left), and spatial profile when focused to a $265 \mu\text{m}$ spot radius (right).

The spectral content of the pulses was measured with a monochromator (ARC, SpectraPro-750). Figure 10 shows a $2.47 \mu\text{m}$ emission peak with 75 nm linewidth (full width at half maximum). Additionally, the predicted atmospheric transmittance over a 2 meter path length [7] is overlaid in black; clearly water absorption features limited spectral content at wavelengths longer than 2500 nm .

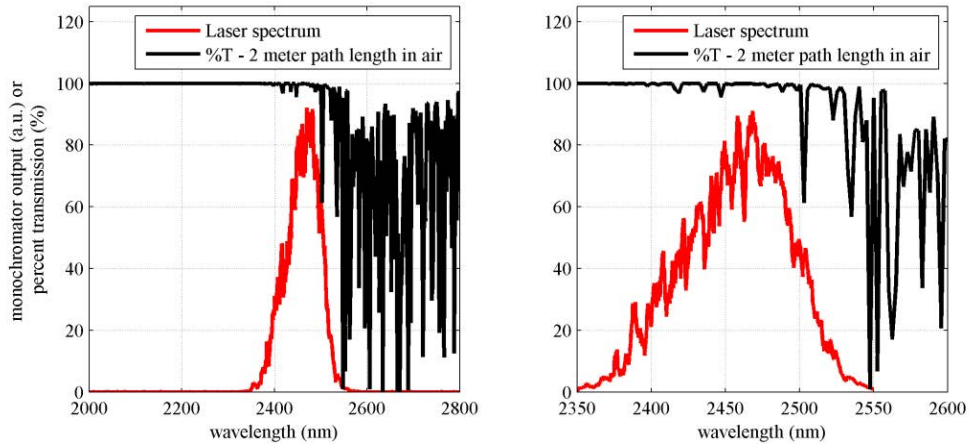


Figure 10. Spectral content of gain-switched $\text{Cr}^{2+}:\text{ZnSe}$ laser output. (left) Complete spectra showing no $2.095 \mu\text{m}$ pump present, (right) zoomed in to show peak emission and linewidth.

3.1.4 Waveguide devices for thermal lensing mitigation

Lasers used for military application will be placed in high stress so they must be compact, rugged and solid-state. Vibration, dust, limited power and large temperature variations are all

issues that must be addressed in any architecture of this type. Free-space laser beam propagation requires optical components such as mirrors, lenses, or gratings to control, re-direct or modulate laser beams. Each component is subject to misalignment and damage due to environmental factors. Approaches that can reduce free-space components are thus highly desirable. Waveguides and fibers are of interest for this reason and for reduced complexity. In addition, waveguides and fibers mitigate thermal issues present in bulk laser and nonlinear materials.

ZnSe has not been fabricated in fiber form nor have waveguides been fabricated in ZnSe, to the best of our knowledge. One method demonstrated in the literature for fabricating optical fibers from crystalline or polycrystalline laser hosts was to use a standard fiber drawing-tower method with a larger diameter, pre-fiber form or *preform* which was constructed using the rod-in-tube (RIT) method [8]. Using this method, a silica rod was tapered at one end and had a hole drilled in the other (see Figure 11). A Cr^{2+} :ZnSe crystal rod doped to the appropriate level was inserted in this hole, which was then capped with silica to contain the crystal. The dimensions of the preform and crystal were designed to give the desired core/cladding size ratio after drawing. The melting point of zinc selenide is 1526°C while the softening point of silica is 1670°C which should have allowed for consistent drawing. The coefficient of thermal expansion of zinc selenide is much higher than that of silica, so heating of the preform was done slowly to avoid thermal shock. Further, it was hoped that the preform could be manufactured to produce modified fiber designs such as a dual-core design to allow pumping in the outer core with signal amplification and guiding in the inner core.



Figure 11. Cr:ZnSe RIT core in silica fiber preform.

The preform was lowered into a drawing tower furnace at Clemson University and a typical drawing routine was followed. The preform subsequently exploded while outside the draw zone which was at 1700° C. The preform had ‘light bulbed’ or blown out into the furnace zone. Due to the nature of zinc selenide, an emergency stop was performed and the room evacuated until the furnace completely cooled. An entire day of cleanup as well as furnace element and heat shield replacement followed.

A separate fiber pull was done with Cr^{2+} :ZnSe powder placed in the tube. In this case fiber was pulled but subsequent measurements showed no signs of Cr^{2+} emission from the fiber. Cr^{2+} emission was observed in parts of the preform that had not been pulled into fiber. Both of these results can be explained by zinc selenide sublimation. Zinc selenide begins sublimating at temperatures below the “drop point” (point at which the fiber can start being pulled) [9] and this is the source of the pressure which caused the explosion of the sealed RIT pull. When using powder, the ZnSe sublimated, moved up the preform to a cooler region and solidified back on the wall of the preform. Thus no ZnSe was incorporated into the fiber core.

We also tried a RIT experiment with a rod that was not sealed with silica on top. This preform also exploded. We believe that, again, the hot end of the rod sublimated to the cool end of the rod. Deposits of ZnSe built up until the rod sealed itself off at the top. Then ZnSe vapor pressure built up until the preform exploded. At this point we declared defeat, since we had no ideas of how to solve the sublimate issue.

We do intend to investigate other fiber or waveguide fabrication techniques. Sazio et al. [10] have developed a process that deposits metals and semiconductors on the surface of a hollow core placed in a silica fiber. The fiber is placed in an oven and reactants are passed through the core region depositing the desired compound on the core surface. Deposition continues until the core fills. Preliminary samples of polycrystalline ZnSe cores have been fabricated for us by Badding's group at Penn State University.

Kar et al. have used ultrashort pulses to fabricate waveguide structures in a variety of materials [11-12]. The ultrashort pulses induce a change in structure at the focus. This change in structure results in a change in refractive index, providing waveguiding. Kar has begun investigation of waveguide fabrication in ZnSe via EOARD Grant FA8655-09-1-3098.

3.2 Development of sub-nanosecond IR source

Pulsed laser radar can use the time of flight of a pulse to measure target distance. Pulse width provides the order-of-magnitude distance resolution possible; actual resolution depends upon pulse shape, signal to noise ratio, etc. A 1 ns pulse is 30 cm long in air. Thus it should be possible to measure target dimensions less than 30 cm using sub-nanosecond pulses and thus provide 3D information for target ID. But target ID systems will need to be used in scenarios where noncombatants are present. For this reason it is preferred to use laser wavelengths in the mid-IR where the ocular maximum permissible exposure (MPE) is 10^5 times higher than it is at visible and near-IR wavelengths which are transmitted by ocular media and focused on the retina. Mid-IR wavelengths are absorbed by the cornea.

3.2.1 Nd μ -chip laser with PPLN frequency conversion

Our first approach was to design, build and demonstrate a compact source using a diode-pumped microchip laser to generate sub-nanosecond pulses. The pulses were then amplified using a fiber amplifier. The main technical issue here was damage to the fiber ends due to the very high peak power generated. This was solved using large diameter (400 μ m) spliced silica end-caps to prevent damage and surfaces polished at 8° to prevent back reflections. The laser and fiber amplifier operated at 1064 nm. Frequency conversion to the mid-IR was done with nonlinear frequency conversion in a periodically poled lithium niobate (PPLN) crystal.

An ytterbium-doped, polarization maintaining (PM) double-clad fiber was seeded at one end and pumped at the other end, using dichroic filters to protect the pump and seed lasers, creating a fiber amplifier. The seed laser was a passively Q-switched, Nd:YAG microchip laser operating at 1064 nm, polarized 99:1, 7.14 kHz repetition rate, 0.5 ns pulse width, average power of 38 mW, and 5.3 μ J pulse energy. The pump laser was a 915 nm diode laser coupled to a fiber pigtail, operating at a maximum of 6 W with 7 A of operating current. The 3.56-m-long FC

connectorized fiber was the active element and had a 25 μm core diameter and a 248 μm inner cladding diameter.

The PPLN crystal was an uncoated 1 x 14 x 49-mm-long multigrating crystal with approximate parallelism of the front and back surfaces. The domain grating period used was 29.5 μm , converting the 720 mW (over 100 μJ pulse energy) fiber amplifier beam to a 1.507 μm signal beam and a 3.619 μm idler beam, with 24% of the pump energy going to the signal and idler outputs.

Further details on performance can be found in publications 3, 11, 12, 13 and 17.

3.2.2 *Tm:YAG μ -chip laser*

An alternative solution to generating sub-nanosecond pulses at infrared eyesafe wavelengths would be to use a microchip laser that operates directly in the infrared spectral region. One possibility not yet considered would be the use of Tm^{3+} as the active lasing ion instead of Nd^{3+} in a μ chip configuration similar to that discussed above for $\text{Nd}^{3+}:\text{YAG}$. Tm also has the advantage that “2 for 1” pumping is possible. Figure 12 shows the energy levels involved in pumping and lasing Tm^{3+} . Pumping from the $^3\text{H}_6$ ground state manifold to the $^3\text{H}_4$ excited state manifold is achievable using commercially available semiconductor lasers operating at 784 nm. One ion excited to the $^3\text{H}_4$ level can then relax by cross-relaxation with another Tm^{3+} ion in the ground state resulting in two ions excited to the intermediate $^3\text{F}_4$ level. Lasing at 2 μm is possible via stimulated emission from the $^3\text{F}_4$ level to the $^3\text{H}_6$ ground state. The “2 for 1” excitation makes this lasing ion very attractive for achieving high efficiency.

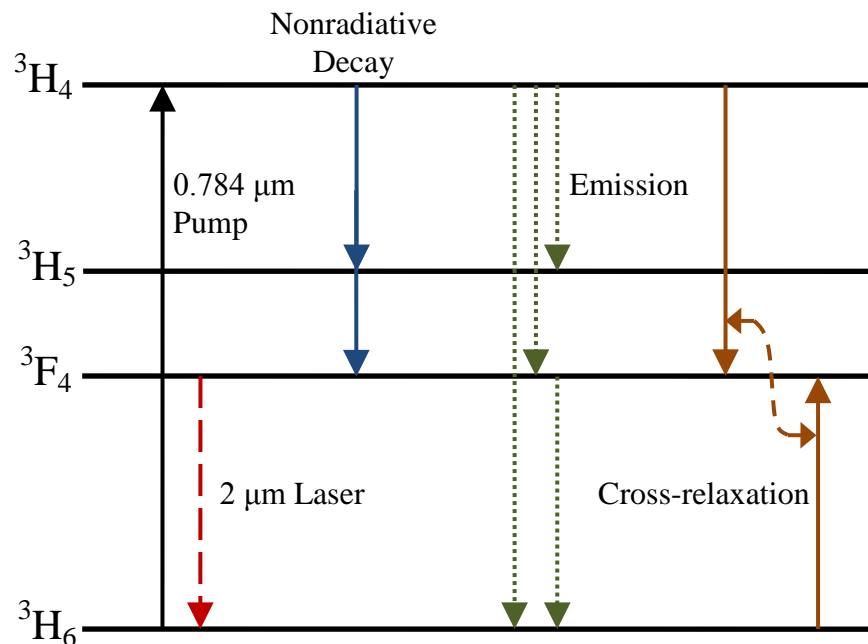


Figure 12. Tm^{3+} energy levels. Each labeled level is actually a manifold of levels split by spin-orbit coupling.

Experimental measurements of $\text{Tm}:\text{YAG}$ absorption are shown in Figure 13. Details of the diode pump absorption region are shown in Figure 14. The peak at 784 nm is the desired pumping point. This peak is similar in bandwidth to the pump laser bandwidth. Since our laser crystals were fabricated to be thin (≤ 2 mm) for short pulse width, this meant that we needed to carefully control the temperature of the diode pump lasers to achieve optimum matching with the absorption peak.

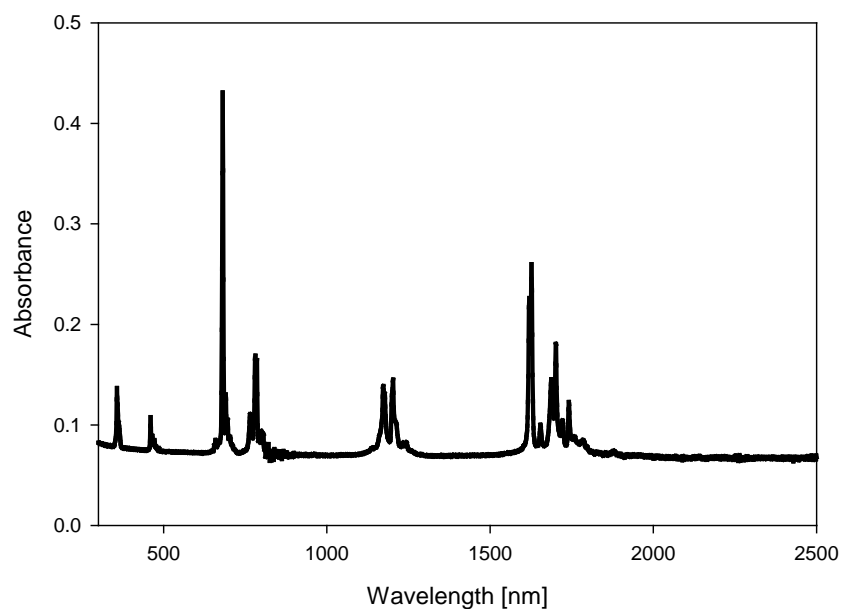


Figure 13. Tm³⁺:YAG absorbance, not corrected for surface reflectivities.

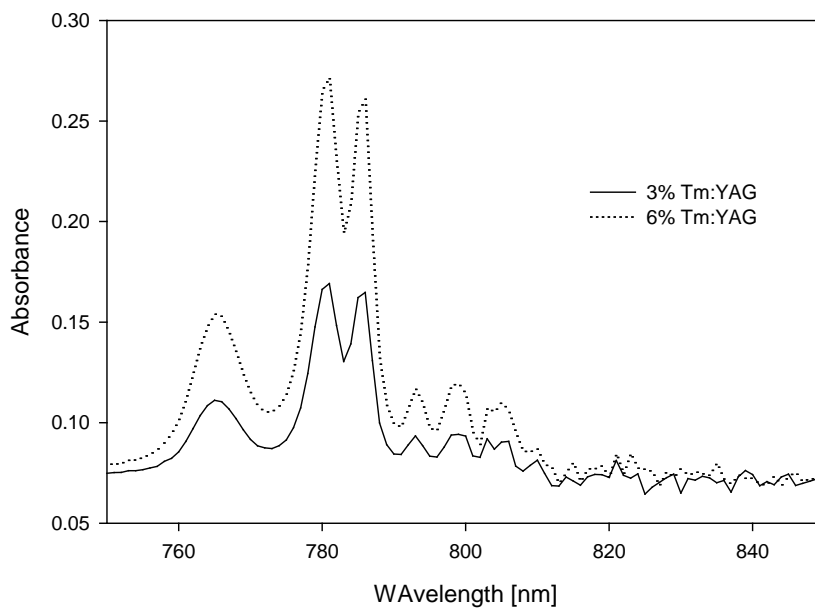


Figure 14. Tm:YAG absorbance in the diode pump region for 3% and 6% Tm doping.

An emission spectrum of Tm:YAG when pumped at 784 nm is shown in Figure 15. The strong emission peak at 2.01 μm is expected to be the lasing wavelength since it represents a transition from the lowest $^3\text{F}_4$ manifold level to a $^3\text{H}_6$ manifold level with low thermal population at room temperature and high cross section.

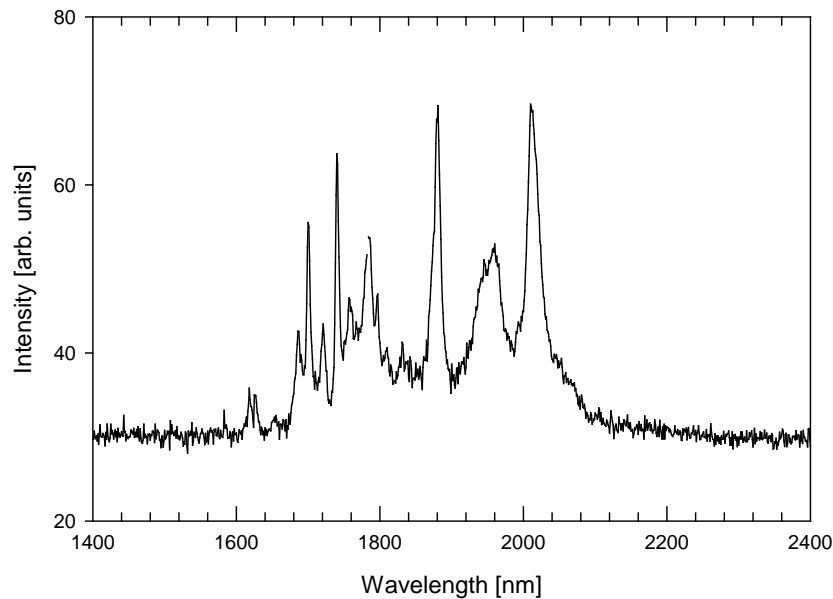


Figure 15. Tm:YAG emission not corrected for spectrometer response.

In contrast to Nd:YAG, Tm:YAG microchip lasers were not commercially available when we began this effort. For that reason we built one ourselves. (A Tm μ chip laser was recently announced for commercial sale; we have ordered one but it has not been delivered yet.) The basic construction (Figure 16) consisted of a thin Tm:YAG crystal which was AR coated at 784 nm for pumping and HR coated at 2 μ m on one side to form one end of a resonator. The other side was AR coated at 2 μ m. A Cr^{2+} :ZnSe AR-coated (@ 2 μ m) slab was inserted to act as a saturable absorber. A partially reflecting mirror provided laser outcoupling.

The oscillator was designed to be as short as possible to provide a short pulse width without concern for pulse energy or efficiency. Amplification is required to increase pulse energy from a few μ J to a few mJ. One way to do this in a robust fashion with minimal free space optics is to use a Tm-doped fiber. A Tm-doped silica core fiber was provided by Defence Science and Technology Organization (DSTO) Australia for our use and evaluation in this project. However, we did not reach the point where we could evaluate the performance of this fiber as an amplifier. Such an effort will be initiated in the future.

Tm:YAG laser crystals were purchased from Onyx Optics. The crystals were doped with 4.2×10^{20} and 8.3×10^{20} ions/cm³ (3 and 6 at%). Samples were fabricated with thicknesses varying from 0.1 mm to 2 mm. The 2 mm thick sample with 6 at% doping achieved the CW laser output shown in Figure 17. The Tm:YAG crystal was pumped by an nLight, 40 W diode laser array with 1.3 nm FWHM bandwidth. The power was coupled to a 400 μ m core fiber. The fiber output was focused with a 4.5 mm focal length lens into the Tm:YAG laser crystal. The output coupler had 99.9% reflectivity at 2 μ m. The output wavelength was 2.019 μ m as measured by a model AQ6375 Yokogawa optical multichannel analyzer. The fiber transported pump beam was highly multimode and the Tm laser output was randomly polarized. Maximum laser output of 450 mW was achieved with about 16 W of diode pump power. This low efficiency was expected

since our laser crystal was so thin. But the oscillator is just intended to serve as the pulse train generator and the fiber amplifier is intended to perform efficient amplification to higher powers.

There is an obvious rollover in slope efficiency as pump power increased (see Figure 17). This is due to the increasing pump power changing the thermal lensing in the resonator thus changing the mode diameter and resonator stability. All of the optical surfaces of the resonator cavity were flat which normally would mean that the resonator is unstable. However, end pumping the Tm:YAG crystal results in heating with generation of a radial thermal gradient. This radial thermal gradient in turn generates a radial refractive index gradient which acts like an optical lens providing resonator stability. Thus the stronger the pump power the stronger the thermal lens becomes. As long as the thermal lens remains much larger than the resonator length the cavity modes should remain stable. Figure 17 shows that we are approaching that limit with pump powers > 10 W.

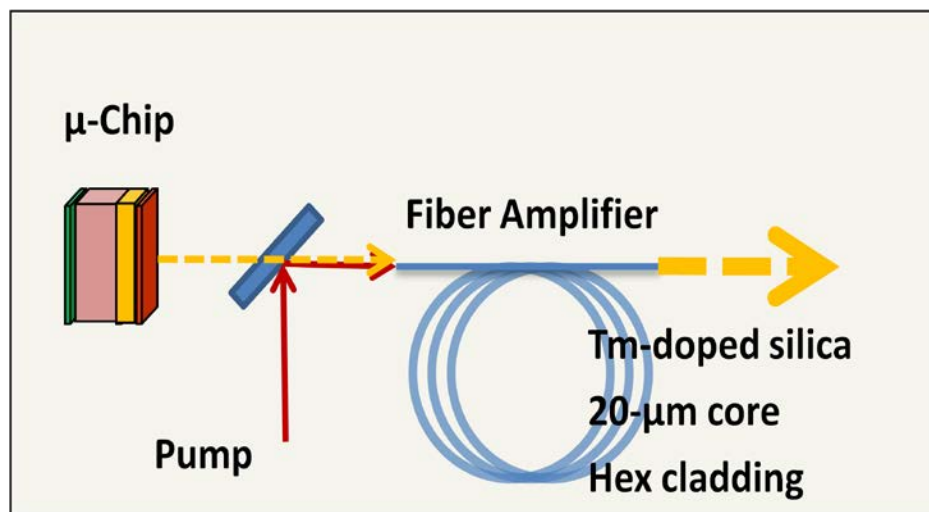


Figure 16. Diagram of 2-μm short pulse laser source.

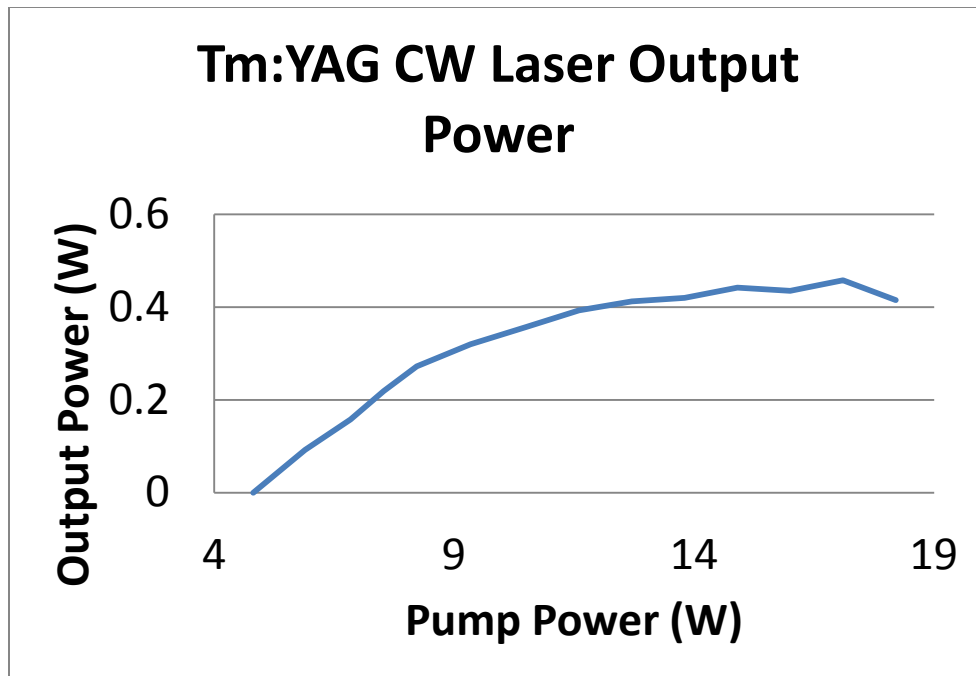


Figure 17. Tm:YAG CW microchip laser power.

Q-switching is a well-known technique for pulsing a laser. There is a variety of methods used to produce this effect, but in all cases some device is inserted into the laser cavity to act as a variable attenuator and introduce additional losses to the cavity. While the laser is being pumped, the attenuation is first increased to the point that the cavity cannot reach its threshold gain (at which point the Q-switch is said to be “closed”), and then is rapidly decreased to immediately induce lasing (where the Q-switch is said to be “open”). The closed Q-switch allows optical pumping to generate a population inversion much higher than achieved with steady-state CW lasing. So there is a large amount of stored energy available for forming a laser pulse. This energy is released in a “giant pulse” which can often reach peak powers orders of magnitude greater than if the same cavity were operating in continuous-wave mode. After the pulse is released, the Q-switch is closed and the cycle repeats.

One method for Q-switching which is especially suitable for microchip and other solid state lasers is to use a saturable absorber in the laser resonator. A saturable absorber is some medium, typically an optically-transparent crystal doped with an absorbing material, that has absorption which is not independent of the incident light intensity. Above a certain intensity most of the absorbers have been excited (saturation of the absorption) and the material becomes more transparent. This change in transparency acts as a Q-switch when it is placed in a resonator. Note that the saturable absorber can be used to Q-switch a laser cavity without requiring any external control (“passive” Q-switching). The process begins with pumping the laser medium and generating photons at the laser wavelength. Here, the saturable absorber is at its highest absorption, which means the cavity losses are also at their maximum. As pumping increases the number of circulating laser photons, the absorption of the Q-switch falls off until cavity losses are smaller than the gain and lasing begins. When the laser pulse is released from the cavity, circulation intensity drops and Q-switch absorption goes back up.

The saturable absorber Q-switch is particularly well-matched to solid state lasers for a few reasons. Most apparently, it's a completely solid state device itself, which makes it both simpler and more robust than other methods of Q-switching. It is completely self-contained, requiring no external power source or modulation. And the Q-switch crystal can often be bonded directly to the laser gain medium, or in some cases the gain medium itself can be doped with the absorbing material, combining gain and pulsing media into one device.

However, passive Q-switching comes with some considerable limitations that preclude it from being the best choice for all pulsing applications; most of these are consequences of device parameters that are fully dependent on the properties of the absorbing material and therefore offer limited adjustability after device fabrication. For example, the pulse rate of a passively Q-switched device cannot be changed without increasing the pump energy, thereby increasing the spontaneous emission rate for laser photons and speeding up the saturable absorber's turnover time. Conversely, the pump energy cannot be changed without affecting the pulse rate. This is not necessarily the case with externally-modulated Q-switching devices. Furthermore, it may prove difficult to find an absorbing material for a wavelength of interest that has otherwise desirable properties. Finally, adding another photonically-active device to a laser system introduces additional phenomenological complexity, making predictive modeling more difficult.

We selected Cr^{2+} -doped ZnSe to be our saturable absorber. $\text{Cr}^{2+}:\text{ZnSe}$ has strong absorption at the 2 μm laser wavelength. $\text{Cr}^{2+}:\text{ZnSe}$ also has a fluorescence lifetime of $\sim 8 \mu\text{s}$ which means Q-switch recovery time from "off" to "on" will be fast allowing multi-kHz pulse repetition rates.

Unfortunately, we were not able to reach lasing threshold using $\text{Cr}^{2+}:\text{ZnSe}$ as a saturable absorber. We suspect that the passive loss (the loss that cannot be saturated or removed through optical pumping) of the absorber was too high. Low power transmission loss of the $\text{Cr}^{2+}:\text{ZnSe}$ saturable absorber was 8% at 2 μm . We also tried using a $\text{Cr}^{2+}:\text{ZnS}$ saturable absorber with a low power transmission loss of 6% at 2.1 μm . This saturable absorber did not achieve lasing either. Q-switched operation has been achieved using an active acousto-optic Q-switch. However, insertion of the Q-switch required enlarging the resonator cavity which reduced average output power and lengthened the Q-switched pulses to several hundred ns, unacceptably long pulses for the intended application.

3.3 Characterization of poled materials using digital image processing

The general idea of nonlinear optical processes in materials is that the incident field strength, \mathbf{E} , induces oscillating dipole moments in each of the atoms. For very high electric fields, the atomic polarization response becomes nonlinear. Due to the nonlinear nature of the response, a polarization, \mathbf{P} , at new frequencies is generated which can radiate at frequencies not present in the incident radiation field. This coupling allows energy to be transferred between different wavelengths and forms the basis of the physical mechanism behind nonlinear frequency conversion.

$$\tilde{P}(t) = \chi^{(1)} \tilde{E}(t) + \chi^{(2)} \tilde{E}^2(t) + \chi^{(3)} \tilde{E}^3(t) + \dots \quad (1)$$

An incident field as shown in Eq. (2),

$$\tilde{E}(t) = E_1 e^{-i\omega_1 t} + E_2 e^{-i\omega_2 t} + c.c., \quad (2)$$

produces the 2nd order polarization shown in Eq. (3),

$$\begin{aligned} \tilde{P}(t) = \chi^{(2)} \left[E_1^2 e^{-2i\omega_1 t} + E_2^2 e^{-2i\omega_2 t} + 2E_1 E_2 e^{-i(\omega_1 + \omega_2)t} + 2E_1 E_2^* e^{-i(\omega_1 - \omega_2)t} + c.c. \right] \\ + 2\chi^{(2)} \left[E_1 E_1^* + E_2 E_2^* \right]. \end{aligned} \quad (3)$$

Note that the resulting polarization has all combinations of ω_1 and ω_2 . These terms represent the possible 2nd order nonlinear interactions.

The nonlinear frequency conversion process requires conservation of energy and conservation of momentum. For example, sum frequency generation requires

$$\begin{aligned} \hbar\omega_3 &= \hbar\omega_1 + \hbar\omega_2 \\ \mathbf{k}_3 &= \mathbf{k}_1 + \mathbf{k}_2 \end{aligned} \quad (4)$$

where $k_i = n(\omega_i) \omega_i / c$. Conservation of momentum can also be considered maintaining a constant phase relationship among the three propagating frequencies. This cannot be done in normal materials due to dispersion, i.e., different frequencies have different phase velocities. The traditional paradigm for achieving phase matching in nonlinear frequency conversion was birefringent phase matching until the mid 1990's. Birefringent materials have different refractive indices for the two orthogonal polarizations of a beam propagating in a given direction. Thus birefringent phase matching may be possible if the right propagation direction (phase matching angle) and right field polarizations are used.

An alternative technique called quasi-phase matching was suggested by Armstrong et al. [13] in 1962. The essential idea of quasi-phase matching is modulation of the nonlinear susceptibility as a function of propagation distance in a crystal. As described with birefringent phase matching above, if $\Delta k \neq 0$ (momentum is not conserved) then the nonlinear interaction goes in and out of phase, the new field to be generated will build up until the phase difference reaches π radians; then the sign of the interaction changes and the frequency conversion goes in the opposite direction and the new field decays back to zero. Hence the new field builds up for one coherence length (l_c) distance over which $\Delta k l_c = \pi$) and then decays for another coherence length. At the point where the field starts to decay, one can flip the nonlinear polarization to essentially set the phase to $-\pi$ and reset the phasing so that the field continues to build up. Then one does another orientation flip at the next coherence length to again reset the sign of the phase and so on. A sign change of the phase is the same as a sign change of the $\chi^{(2)}$ coefficient. Such a flip can be accomplished by changing the orientation of the nonlinear material being used. The $\chi^{(2)}$ interaction can be represented by a 2nd order tensor. Rotation of a tensor (by rotating the crystal orientation) results in changes in the signs of its components. By spacing these sign changes by one coherence length, the field will grow, although at a slower rate than perfect phase matching.

All of this was moot for over 30 years because no one could figure out a way to fabricate such a crystal with precise changes of orientation every coherence length; and coherence lengths are typically 10's of μm 's. But a major breakthrough came when researchers discovered that ferroelectric materials could be reoriented through electric field poling [14]. Electric field poling induces an ion shift in ferroelectric materials that is equivalent to a 180° rotation that changes the sign of $\chi^{(2)}$. Periodically poled lithium niobate (PPLN) was shown to have excellent nonlinear frequency conversion properties.

Once periodically poled nonlinear crystals could be produced, there was a need to evaluate and improve their performance. Quality of poling can vary significantly from crystal to crystal and between different regions in the same crystal. Observation of the poled domains with a microscope is possible, after etching a poled surface with a solution that has different rates of etch for the $z+$ and $z-$ surfaces. But such a technique is very qualitative with only a general ability to label PPLN crystals as “good” or “bad”. It is also possible to evaluate poled crystals by placing them in a test frequency conversion setup and comparing the observed frequency conversion efficiency to theory and to a standard or “best” crystal. But this requires considerable time to do the analysis and involves major equipment investment to purchase and maintain the test setup.

We investigated a new poling quality evaluation approach based on image processing across an entire $z+$ or $z-$ surface of a poled crystal (Publication 17). This process allows for better quantification of the underlying domain structure and directly relates to device performance. The poled regions were determined from images taken with a microscope and this mapping was then used to determine an effective nonlinear $\chi^{(2)}$ coefficient (also known as d -coefficient, $2d = \chi^{(2)}$).

3.3.1 Methodology

The main steps for this evaluation technique were

- (a) to obtain an image of the entire crystal
- (b) to map the crystal domains by determining the positions of the domain boundaries through image processing
- (c) to calculate the modified effective nonlinear coefficient, d_{eff} , and then
- (d) to compare it to measurements based on an OPG setup.

To map the crystal domains of a periodically poled material, pictures of an entire $z+$ or $z-$ face were acquired. This was accomplished by taking a series of slightly overlapping pictures (using a motorized stage or manually) using a reasonably high magnification optical microscope (Nikon AZ-100). Some software packages will combine this into a single image resulting in a single massive file, but such a large file can be difficult to use. An alternative is to calculate how to align the pictures by registering them together. A feature-based registration technique was appropriate for our application since poling imperfections and dirt in the overlapping regions could be used as features for aligning. The translation was determined for all images relative to the first image.

A representative microscope image is shown below in Figure 18. A sampled radial Gaussian function filtering technique was first used to smooth features smaller than a particular size. Next partial derivatives were used to extract locations of the domain boundaries. Then a line detection routine was used to connect the domain boundary dots. Linear interpolation was used to fill in any gaps. The result is as shown in Figure 19. Black is for a negative d-coefficient and white is for a positive d-coefficient.

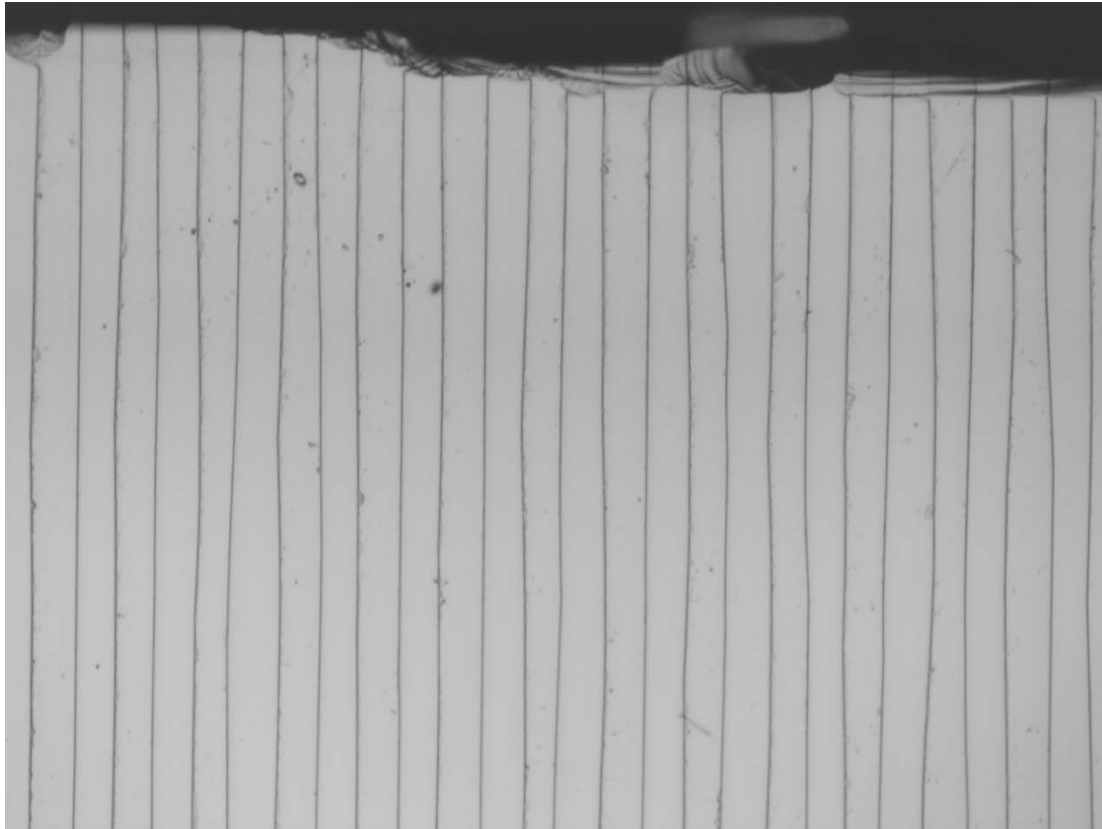


Figure 18. Typical etched lithium niobate test sample image.

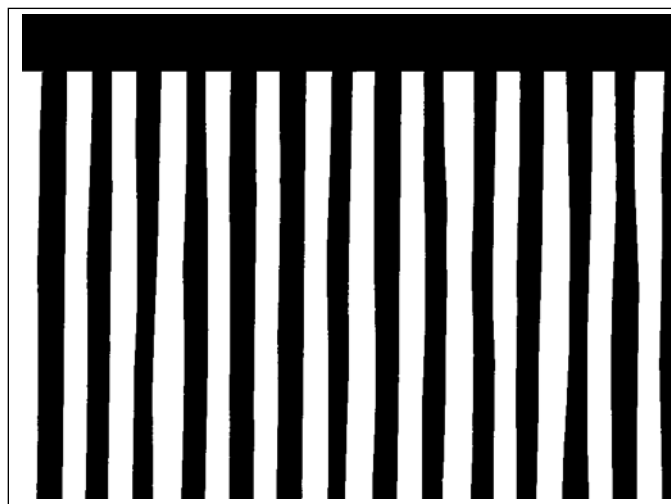


Figure 19. Binary map of domain structure.

Using row 1000 as an example, the Fourier transform of the binary map is shown in Figure 20, for different levels of zero-padding. Zero-padding is adding extra zeros at the end of the array of numbers to be transformed, which increases the resolution in spatial frequency space. The higher amounts of zero-padding give the most accurate value of the lowest frequency peak in the Fourier transform. The Fourier transform d-coefficient is calculated for every row in an image and for every image so we end up with a matrix of d-coefficients that describe the relative poling quality at various locations in the crystal. Note that this technique cannot give us the absolute magnitude of the d-coefficient but gives us relative magnitudes for different locations.

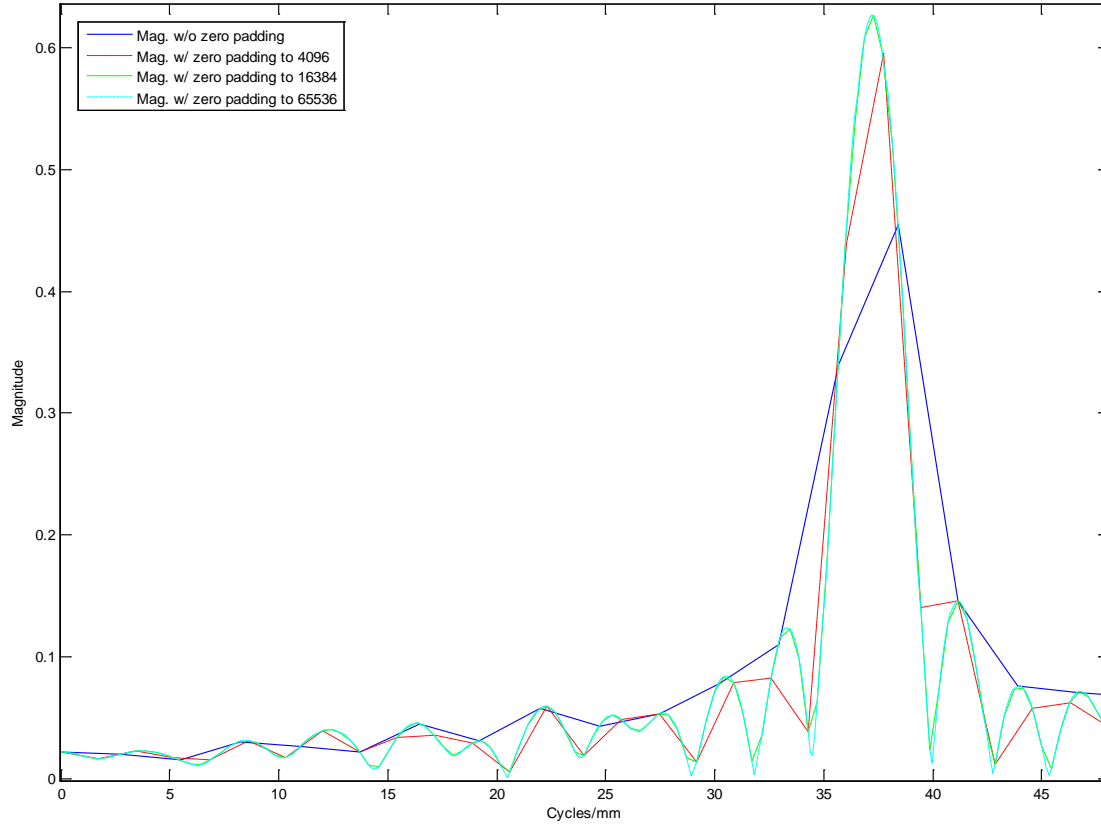


Figure 20. Fourier transform of map at row 1000 using various levels of zero-padding.

The average effective d-coefficient value can then be calculated for a particular pump beam used in a nonlinear conversion process. To test our image processing results, we set up an OPG (optical parametric generation) experiment.

3.3.2 Experimental OPG test

A 1.064 μm wavelength laser beam was used to pump the PPLN crystal that had been characterized for d-coefficient values vs. beam location using the above image processing methodology. After aligning the crystal for efficient conversion by ensuring that the back reflections were collinear with the incident beam, the signal and idler were directed to an energy meter for measurement. At this orientation, the Fresnel reflections from the crystal facets lead to a low-finesse monolithic OPO which slightly lowers the threshold as compared to when the

crystal is rotated away from the resonant condition. To determine the threshold, the pump energy was adjusted until the combined signal and idler energy reached $1\mu\text{J}$. The pump energy was measured when that condition was met and then the whole process was repeated several times while translating the crystal laterally relative to the pump beam. The crystal's performance was compared to the prediction based on mapping domain boundaries of the entire crystal top surface. The measured and calculated pump threshold across the width of the crystal is shown in Figure 21. Since the calculation was relative, the constant of proportionality was adjusted until the scale of the calculated threshold matched the measured thresholds visually.

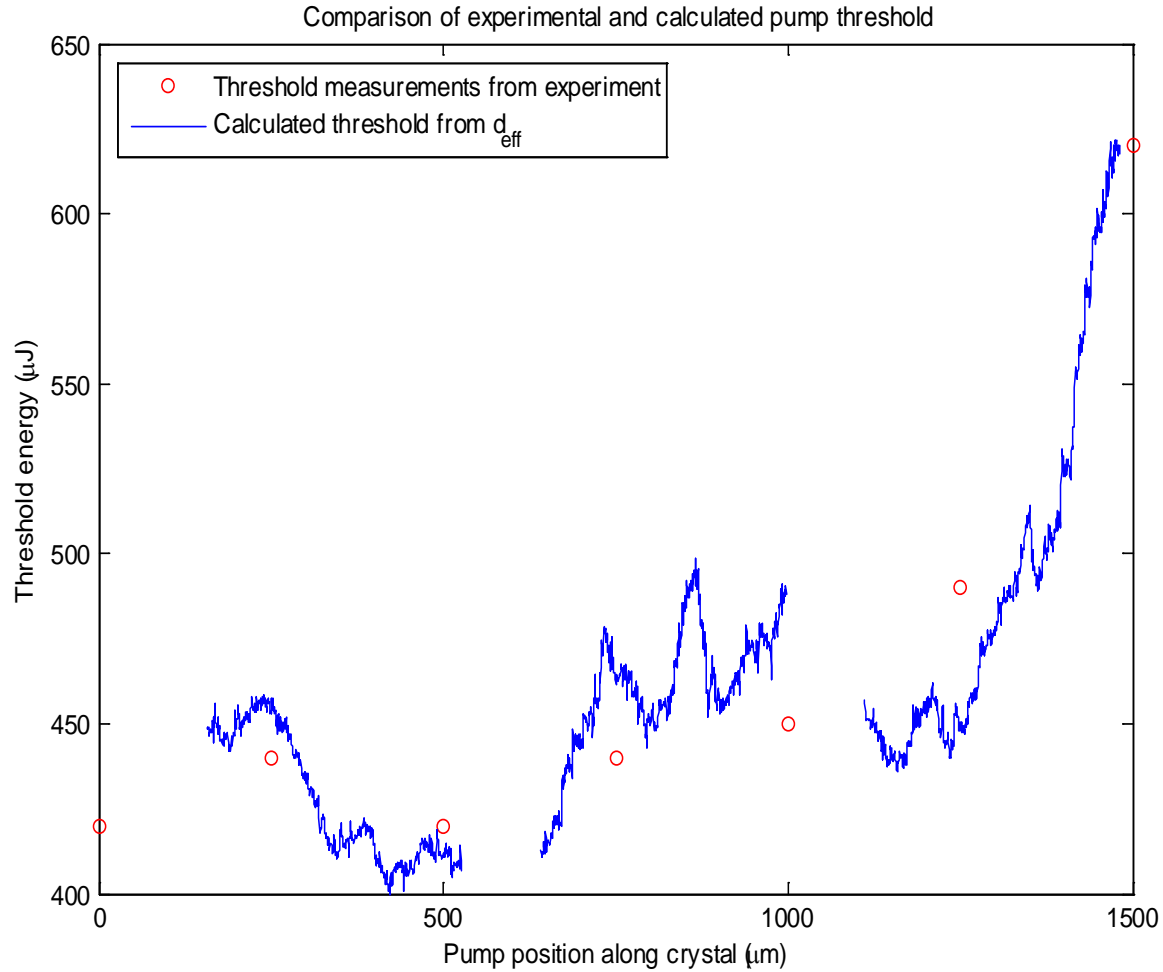


Figure 21. Calculated and measured threshold of PPLN crystal in an OPG setup.

The full PPLN crystal surface was comprised of 38 columns by 3 rows of images. The columns were registered relative to each other but the rows were not due to a lack of sufficient row-to-row overlap; this leaves the gaps shown in the 500 and 1000 μm crystal positions.

3.3.3 Image processing conclusions

A technique for quantitatively evaluating the poling quality of quasi-phase matched crystals has been demonstrated. After stitching a mosaic of microscope images together, the locations of crystal domains were accurately determined through a series of imaging processing steps. The full crystal map was used to calculate a relative d_{eff} and then subsequently was compared experimentally to an OPG threshold measurement as a function of position in the crystal. The mapping of d_{eff} to threshold matched the OPG measurements quite well, validating this method as a useful means to evaluate nonlinear optical crystal performance. Beyond this proof of concept, the data extracted from the images could easily be applied to other processes like second harmonic generation and be used for any laser wavelength. The technique should be applicable to other QPM materials such as OPGaAs too. Future improvements in the QPM fabrication process should be possible by using this technique to produce quantifiable metrics to compare device fabrication iterations without resorting to full device testing, which has applications in Quality Assurance as well as device development.

4. Conclusions

The following points summarize the key accomplishments and significant conclusions that can be drawn from the current program:

1. $\text{Cr}^{2+}:\text{ZnSe}$ laser power was scaled up to 14 W CW in a MOPA configuration which simultaneously provides high power and high beam quality.
2. Tunable $\text{Cr}^{2+}:\text{ZnSe}$ lasing over a 400 nm range (2275-2700 nm) was achieved with grating tuning and powers ranging from 2 to 9 W.
3. Passive saturable absorber modelocking was achieved with several hundred mW of output power.
4. Gain switched lasing of $\text{Cr}^{2+}:\text{ZnSe}$ generated 3 mJ of output energy with 52% slope efficiency. The pump laser pulse width (FWHM) was 90 ns and generated two $\text{Cr}^{2+}:\text{ZnSe}$ pulses within that envelope; the primary peak has a 10 ns FWHM.
5. Efforts to fabricate a $\text{Cr}:\text{ZnSe}$ fiber core using the RIT method were unsuccessful. More promising techniques include deposition of ZnSe in the hollow core of a silica fiber and fabrication of waveguide structures in ZnSe using ultrashort pulses.
6. Sub-nanosecond pulses were generated using a μ -chip Nd laser oscillator and a ytterbium-doped, PM double-clad fiber. Wavelengths were converted to the mid-IR using nonlinear OPG in a PPLN crystal.
7. An alternative solution to generating sub-nanosecond pulses at infrared eyesafe wavelengths was investigated. This consisted of a $\text{Tm}:\text{YAG}$ microchip laser that operates directly in the infrared spectral region at 2 μm and amplification with a Tm -doped silica fiber. CW Tm lasing was achieved but passive Q-switched was not, probably due to use of a saturable absorber with non-saturable loss that was too high.
8. A technique for quantitatively evaluating the poling quality of quasi-phase matched crystals has been demonstrated. Image processing of PPLN domains was used to calculate a relative d_{eff} and then subsequently was compared experimentally to an OPG threshold measurement as a function of position in the crystal. The mapping of d_{eff} to threshold matched the OPG measurements quite well.

5. Recommendations

1. Expand investigation of tunable mid-IR lasers to include $\text{Fe}^{2+}:\text{ZnSe}$. $\text{Fe}^{2+}:\text{ZnSe}$ has been shown to have broadband lasing in the 3.5-5 μm region. All of the work that has gone into developing $\text{Cr}^{2+}:\text{ZnSe}$ should be easily transitioned to $\text{Fe}^{2+}:\text{ZnSe}$. The two laser materials can cover most of the mid-IR spectral region
2. Further investigate the fabrication of $\text{Cr}^{2+}:\text{ZnSe}$ fibers and waveguides. Demonstrate $\text{Cr}^{2+}:\text{ZnSe}$ fiber/waveguide lasers which should be scalable to high powers because thermal lensing will no longer be an issue.
3. Further investigate high-power modelocking in $\text{Cr}^{2+}:\text{ZnSe}$ and extend it to $\text{Fe}^{2+}:\text{ZnSe}$.
4. Use a tunable, gain-switched $\text{Cr}^{2+}:\text{ZnSe}$ laser to pump an OPGaAs OPO. A small range of pump laser tuning in the 2.5- μm region can provide a very wide range of OPO output. Electronic tuning of pump wavelength with a piezo device would make the tuning rate extremely fast.
5. Synchronously pump a QPM device, such as an OPGaAs OPO to efficiently generate 8-12 μm output.
6. Couple lasing and nonlinear frequency conversion in the same chip using, for example, waveguides fabricated in orientation patterned $\text{Cr}^{2+}:\text{ZnSe}$.
7. Further investigate and improve the performance of the Tm μ -chip laser. Co-doping with Ho, which has higher gain, could reduce threshold and improve efficiency.
8. The image processing technique for characterizing the quality of the domain patterning in PPLN should be applicable to other QPM materials such as OPGaAs too. Future improvements in the QPM fabrication process should be possible by using this technique to produce quantifiable metrics to compare device fabrication iterations without resorting to full device testing. However, this is more likely to be an issue for industry when high quality and high volume production are needed.

6. References

- [1] James R. Alverson, "Characterization of periodically poled nonlinear materials using digital image processing," AFRL-RY-WP-TM-2008-1205 (April 2008).
- [2] L. D. DeLoach, R. H. Page, G. D. Wilke, S. A. Payne, and W. F. Krupke, "Transition metal-doped zinc chalcogenides: spectroscopy and laser demonstration of a new class of gain media," *IEEE Journal of Quantum Electronics*, **32**(6): 885-895 (1996).
- [3] S. B. Mirov, V. V. Fedorov, I. S. Moskalev, and D. V. Martyshkin, "Recent Progress in Transition-Metal-Doped II-VI Mid-IR Lasers," *IEEE Journal of Selected Topics in Quantum Electronics*, **13**(3): 810-822 (2007).
- [4] T. J. Carrig, G. J. Wagner, A. Sennaroglu, J. Y. Jeong, C. R. Pollock, "Mode-locked Cr^{2+} :ZnSe laser," *Optics Letters* **25**: 168-170. (2000).
- [5] I. T Sorokina, E. Sorokin, and T. J Carrig, "Femtosecond pulse generation from a SESAM mode-locked Cr:ZnSe laser," CLEO/QELS Technical Digest on CD, paper CMQ2, Long Beach, CA, Optical Society of America (2006).
- [6] C. Hoenninger, R. Paschotta, F. Morier-Genoud, M. Moser, and U. Keller, "Q-switching stability limits of continuous-wave passive mode locking," *Journal of the Optical Society of America B* **16**: 46-56 (1999).
- [7] S. T. Fiorino, R. J. Bartell, M. J. Krizo, G. L. Caylor, K. P. Moore, T. R. Harris, and S. J. Cusumano, "A first principles atmospheric propagation & characterization tool-the laser environmental effects definition and reference (LEEDR)," in *SPIE Atmospheric Propagation of Electromagnetic Waves II* (2008).
- [8] Y.-C. Huang, Y.-K. Lu, J.-C. Chen, Y.-C. Hsu, Y.-M. Huang, S.-L. Huang, and W.-H. Cheng, "Broadband emission from Cr-doped fibers fabricated by drawing tower," *Optics Express* **14**, 8492-8497 (2006).
- [9] M. S. Hassan, and Z. A. Munir, "Studies on the Sublimation of IIB-VIA Compounds. VI. Thermodynamics of the Dissociation of Zinc Selenide," *High Temperature Science* **5**, 34-39 (1973).
- [10] P. J. A. Sazio, A. Amezcua-Correa, C. E. Finlayson, J. R. Hayes, T. J. Scheidemantel, N. F. Baril, B. R. Jackson, D.-J. Won, F. Zhang, E. R. Margine, V. Gopalan, V. H. Crespi, and J. V. Badding, "Microstructured Optical Fibers as High-Pressure Microfluidic Reactors," *Science* **311**, 1583-1586 (2006).
- [11] A. Benayas, W. F. Silva, A. Ródenas, C. Jacinto, J. V. d. Aldana, F. Chen, Y. Tan, R. R. Thomsom, N. D. Psaila, D. T. Reid, G. A. Torchia, A. K. Kar, and D. Jaque, "Ultrafast laser writing of optical waveguides in ceramic Yb:YAG: a study of thermal and non-thermal regimes," *Applied Physics A* in press, (2010).

- [12] R. R. Thomson, S. Campbell, I. J. Blewett, A. K. Kar, D. T. Reid, S. Shen, and A. Jha, "Active waveguide fabrication in erbium-doped oxyfluoride silicate glass using femtosecond pulses," *Applied Physics Letters* **87**, 1211021-1211023 (2005).
- [13] J.A. Armstrong, N. Bloembergen, J. Ducuing, and P.S. Pershan, "Interactions between light waves in a nonlinear dielectric." *Physical Review* **127**:1918-1925 (1962).
- [14] L. E. Myers, R. C. Eckardt, M. M. Fejer, R. L. Byer, W. R. Bosenberg, and J. W. Pierce, "Quasi-phase-matched optical parametric oscillators in bulk periodically poled LiNbO₃," *Journal of the Optical Society of America B* **12**, 2102-2116 (1995).

7. List of Publications and Presentations

Based in Whole or in Part on Results from the Current Program

Publications:

1. P. A. Berry and K. L. Schepler, "High-power, widely-tunable Cr^{2+} :ZnSe master oscillator power amplifier systems," *Optics Express*, **18**, No 14, 15062-15072 (2010).
2. Matthew D. Cocuzzi, Kenneth L. Schepler, and Peter E. Powers "Narrow-bandwidth, subnanosecond, infrared pulse generation in PPLN pumped by a fiber amplifier–microchip oscillator," *IEEE Journal of Selected Topics in Quantum Electronics*, **Vol 15**, No 2, 372-376 (2009).
3. R. K. Shori, K. L. Schepler, and W. A. Clarkson, editors, *Progress in Solid-State, Fiber, and Tunable Sources*, IEEE Journal of Selected Topics in Quantum Electronics, **Vol 13**, No 3, May/June 2007.
4. Larry D. Merkle, Mark Dubinskii, Kenneth L. Schepler, and S. M. Hegde, "Concentration quenching in fine-grained ceramic Nd:YAG," *Optics Express*, **14** (9), 3893-3905 (2006).
5. V. Gopalan, K. L. Schepler, V. Dierolf, and I. Biaggio, "Ferroelectric Materials," chapter in *The Handbook of Photonics*, Second Edition, Mool C. Gupta and John Ballato, editors, CRC Press, 2006.

Conference Presentations/Papers:

6. V.V. Fedorov, I.S. Moskalev, M.S. Mirov, S.B. Mirov, T.J. Wagner, M.J. Bohn, P.A. Berry and K.L. Schepler, "Energy scaling of nanosecond gain-switched Cr^{2+} :ZnSe lasers," accepted for presentation at (SPIE) Photonics West 2011, San Francisco, California, USA, 2011.
7. P.A. Berry, and K.L. Schepler, " Cr^{2+} :ZnSe master oscillator / power amplifier for improved power scaling," Solid State Lasers XIX: Technology and Devices, Vol 7578, 75781L:1-11. (SPIE) Photonics West 2010, San Francisco, California, USA, 2010.
8. P.A. Berry, and K.L. Schepler, "High-Power, Widely Tunable Cr^{2+} :ZnSe Laser," in Conference on Lasers and Electro-Optics (Optical Society of America, San Jose, CA, 2010).
9. Igor S. Moskalev, Vladimir V. Fedorov, Sergey B. Mirov, Patrick A. Berry, and Kenneth L. Schepler, "12-Watt CW Polycrystalline Cr^{2+} :ZnSe Laser Pumped by Tm-Fiber Laser," presented at Advanced Solid State Photonics, Denver CO, Feb 2009 (Optical Society of America).

10. Matthew D. Cocuzzi, Charles D. Phelps, Kenneth L. Schepler, and Peter E. Powers, "Fiber-guided seeding of narrow bandwidth, sub-nanosecond optical parametric pulse generation in PPLN," IEEE LEOS 21st Annual Meeting Proceedings, pp. 878-879, Long Beach CA, Nov 2008.
11. Matthew D. Cocuzzi, Patrick Berry, and Kenneth L. Schepler, "Fiber amplifier optical parametric generation in PPLN for high-resolution laser radar," presented at the MSS Active EO Conference 2008, San Diego CA.
12. Matthew D. Cocuzzi, Kenneth L. Schepler, Peter E. Powers, and Ivan T. Lima, Jr., "Sub-nanosecond infrared optical parametric pulse generation in PPLN pumped by a seeded fiber amplifier," paper WB30 presented at *Advanced Solid-State Photonics* in Nara Japan, Feb 2008 (Optical Society of America).
13. Kenneth L. Schepler, "Mid-IR transition metal lasers," in Solid State Lasers XVI: Technology and Devices, Proceedings of SPIE Volume 6451 (SPIE, Bellingham, WA, 2007) 64510K.
14. Kenneth L. Schepler, Rita D. Peterson, and Patrick A. Berry, "Scaling Mid-infrared Cr²⁺ Laser Operation to High Powers," Great Lakes Photonics Symposium, Paper GL107-09 (2006).
15. Patrick A. Berry and Kenneth L. Schepler, "Modeling of time-dependent thermal effects in Cr²⁺-doped zinc selenide thin disks, Proc. of SPIE Vol 6100, (2006) 61000X1-10.

Technical Reports:

16. Matthew D. Cocuzzi, "Sub-nanosecond infrared optical parametric pulse generation in periodically poled lithium niobate pumped by a seeded fiber amplifier," AFRL-RY-WP-TR-2008-1033 (February 2008).
17. James R. Alverson, "Characterization of periodically poled nonlinear materials using digital image processing," AFRL-RY-WP-TM-2008-1205 (April 2008).
18. Patrick A. Berry, "Versatile chromium-doped zinc selenide infrared laser sources," AFRL-RY-WP-TR-2010-1107 (May 2010).

8. List of Acronyms, Abbreviations, and Symbols

Acronym/ Abbreviation	Description
AFOSR	Air Force Office of Scientific Research
AFRL	Air Force Research Laboratory
AR	Anti-Reflective
CW	Continuous Wave
DoD	Department of Defense
DSTO	Defence Science and Technology Organization
FROG	Frequency Resolved Optical Gating
FWHM	Full Width at Half Maximum
HR	Highly Reflective
ID	Identification
IRCM	Infrared Countermeasures
MOPA	Master Oscillator Power Amplifier
MPE	Maximum Permissible Exposure
Mid-IR	mid-infrared wavelengths (2-5 μm wavelengths)
MURI	Multidisciplinary University Research Initiative
NRL	Naval Research Laboratory
OC	Output Coupler
OEMs	Original Equipment Manufacturers
OPG	Optical Parametric Generation
OPGaAs	orientation-patterned gallium arsenide
OPO	Optical Parametric Oscillator

PPLN	periodically poled lithium niobate
PM	Polarization Maintaining
PRDA	Program Research and Development Announcement
QPM	Quasi Phase Matching
ROC	Radius of Curvature
RIT	Rod-In-Tube
SA	Saturable Absorber
SEO	Schwartz Electro-Optics
SESAM	semiconductor saturable absorber mirror
SFG	Sum Frequency Generation
USAF	United States Air Force
WU	Work Unit
YAG	yttrium aluminum garnet

Symbol	Description
α	absorption coefficient
at%	atomic percent doping
Cr	chromium
Cr^{2+}	chromium ion with 2 ⁺ valency
dn/dT	change in refractive index with change in temperature
η	efficiency
Er	erbium
Fe	iron

h	Planck constant
Ho	holmium
μ -chip	micro-chip
μm	micron (10^{-6} m)
n	refractive index
Nd	neodymium
σ	cross section
Se	selenium
S/N	Signal-to-noise ratio
Tm	thulium
$\chi^{(n)}$	n^{th} order nonlinear coefficient
Zn	zinc